A Sensorless Power Reserve Control Strategy for Two-Stage Grid-Connected PV Systems

Sangwongwanich, Ariya; Yang, Yongheng; Blaabjerg, Frede

Published in:
IEEE Transactions on Power Electronics

DOI (link to publication from Publisher):
10.1109/TPEL.2017.2648890

Publication date:
2017

Document Version
Accepted author manuscript, peer reviewed version

A Sensorless Power Reserve Control Strategy for Two-Stage Grid-Connected PV Systems

Ariya Sangwongwanich, *Student Member, IEEE,* Yongheng Yang, *Member, IEEE,* and Frede Blaabjerg, *Fellow, IEEE*

***Abstract*—Due to the still increasing penetration of grid-connected Photovoltaic (PV) systems, advanced active power control functionalities have been introduced in grid regulations. A power reserve control, where namely the active power from the PV panels is reserved during operation, is required for grid support. In this paper, a cost-effective solution to realize the power reserve for two-stage grid-connected PV systems is proposed. The proposed solution routinely employs a Maximum Power Point Tracking (MPPT) control to estimate the available PV power and a Constant Power Generation (CPG) control to achieve the power reserve. In this method, the solar irradiance and temperature measurements that have been used in conventional power reserve control schemes to estimate the available PV power are not required, and thereby being a sensorless approach with reduced cost. Experimental tests have been performed on a 3-kW two-stage single-phase grid-connected PV system, where the power reserve control is achieved upon demands.**

***Index Terms*—Active power control, power reserve control, maximum power point tracking, constant power generation control, PV systems, grid-connected power converters.**

I. Introduction

In recent decades, the penetration level of Photovoltaic (PV) systems has been continuously increasing, especially for grid-connected applications [1]–[5]. Due to the still declining installation costs (e.g., in PV panels and inverters), grid-connected PV systems will have an even more significant role in the future power production [2], [3]. This makes the power grid to be mixed in terms of energy resources, and thereby increases the control and monitoring complexity. As a consequence, grid regulations have recently been revised and continuously updated in order to handle the increased amount of fluctuating PV power injected to the power grid [5]–[9]. Several advanced active power control strategies have been defined [4]–[9], where the PV system is expected to be more active in the power network beyond a purely power-generating unit. One of the advanced functionalities in grid-connected PV systems is to reserve active power for potential grid voltage or frequency regulations [4], [7]–[9], where a certain amount of active power is reserved (or curtailed) during operation. Fig. 1 gives an example of the power reserve control requirement in the Danish grid code [7]. Typically, the Power Reserve Control (PRC) can be adopted for potential frequency regulation during a short period (e.g., frequency response) [6]–[11].

Manuscript received September 1, 2016; revised November 10, 2016; accepted December 29, 2016. This work was supported in part by the European Commission within the European Union's Seventh Frame-work Program (FP7/2007-2013) through the SOLAR-ERA.NET Transnational Project (PV2.3 - PV2GRID), by Energinet.dk (ForskEL, Denmark, Project No. 2015-1-12359), and in part by the Research Promotion Foundation (RPF, Cyprus, Project No. KOINA/SOLAR-ERA.NET/0114/02). Corresponding Author: Yongheng Yang.

The authors are with the Department of Energy Technology, Aalborg University, DK-9220 Aalborg, Denmark (e-mail: ars@et.aau.dk; yoy@et.aau.dk; fbl@et.aau.dk).

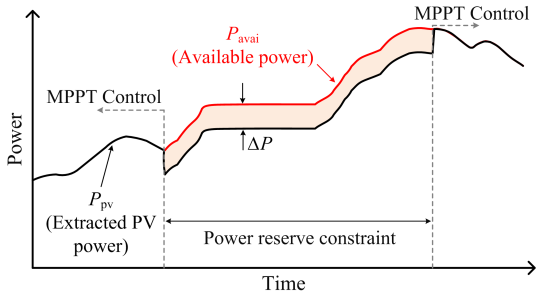

Fig. 1. Power reserve requirement in the Danish grid code [7], where ΔP is the amount of power reserve level.

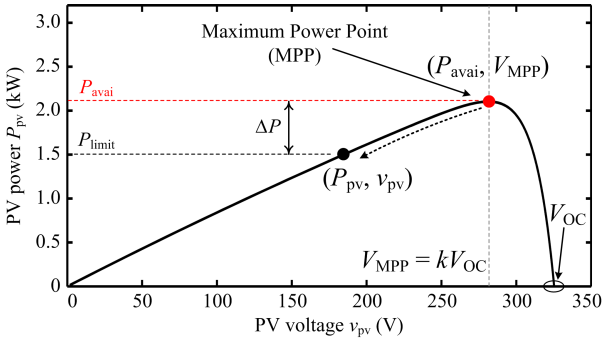

Fig. 2. Power-voltage curve of the PV panels with the power reserve control by operating the PV system at below the MPP.

Energy storage devices (e.g., battery) are normally employed to realize the power reserve in PV systems [11]–[16]. However, high cost and limited lifetime are the two main drawbacks, which makes this solution not so cost-effective, and also becoming the main driving forces for advanced control solutions with reduced cost and complexity [10]. As an alternative, the power reserve can be achieved by modifying the control algorithm of the PV system to operate below the Maximum Power Point (MPP), and then the active power can be reserved [17]–[21]. In order to do so, the modified MPPT algorithm has to be able to regulate the PV power P_{pv} at a certain power limit P_{limit}, as it has been proposed in [10]–[12] and illustrated in Fig. 2. To achieve the PRC strategy, the set-point P_{limit} has to be calculated by subtracting the available PV power P_{avai} with the required amount of power reserve ΔP as

$$P_{pv} = P_{limit} = P_{avai} - \Delta P. \tag{1}$$

Usually, the reserved power ΔP is calculated as a function of the frequency deviation or given by the system operators [10]–[12]. In that regard, it is considered as an input (or reference) for the PRC strategy. Thus, the remaining issue becomes clear - how to accurately estimate the available PV power P_{avai} during operation [22]. The estimation is very challenging [23], unless the PV system is equipped with an accurate irradiance measurement as implemented in [10] and [11]. However, this is usually not the case for residential/commercial scale PV systems, since the irradiance measurements will increase both the cost and the complexity of the overall system. In contrast, the method proposed in [12] and [23] uses a quadratic curve-fitting approach to estimate the available PV output power from the Power-Voltage (P-V) curve of the PV panels, without using an irradiance measurement. However, it requires the estimation of the PV voltage at the MPP, V_{MPP}, which incurs additional efforts. Besides, the accurate estimation of the curve-fitting approach is limited to a certain range (i.e., $v_{\text{pv}} < V_{\text{MPP}}$) and the method is also sensitive to parameter variations (e.g., due to aging of PV panels).

In light of the above issues, it calls for a cost-effective and simple solution to realize the PRC strategy. This paper thus proposes a Sensorless Power Reserve Control (SPRC) strategy to fill out this gap, where the solar irradiance measurements are not required for the available PV power estimation. The proposed solution routinely employs the MPPT operation to measure the available PV output power, which is simple and more generic [24]. Then, the PV output power is regulated according to the required amount of power reserve by means of a CPG strategy [17], [18]. At the grid-side converter, the stored energy in the dc-link is also adaptively controlled to buffer the PV power increase during the MPPT operation, and thereby keep the injected ac power to follow the required power reserve profile. The proposed approach can overcome the limitation in [25], where the PRC constraint cannot be maintained during the MPPT operation.

The rest of this paper is organized as follows: the system description and the overall control structure of two-stage PV systems is presented in Section II. In Section III, the operational principle of the proposed SPRC strategy is discussed, and the design considerations are provided in Section IV. Experimental tests have been carried out on a 3-kW two-stage single-phase grid-connected PV system in Section V to verify the effectiveness of the proposed strategy. Finally, Section VI gives the concluding remarks.

II. System Description of Two-Stage PV Systems

The system configuration of a two-stage grid-connected PV systems is shown in Fig. 3. This two-stage configuration is widely used in the residential/commercial PV systems (e.g., with the rated power of 1-30 kW) [26], [27], where it consists of two power converters: 1) the PV-side dc-dc boost converter and 2) the grid-side dc-ac inverter. Basically, the boost converter is responsible for extracting the PV power P_{pv}, which is achieved by regulating the PV voltage v_{pv} at the corresponding operating point in the Power-Voltage (P-V) curve in Fig. 2, e.g., at the V_{MPP} for the MPPT operation. Then, the grid-side converter, which is realized by a full-bridge topology,

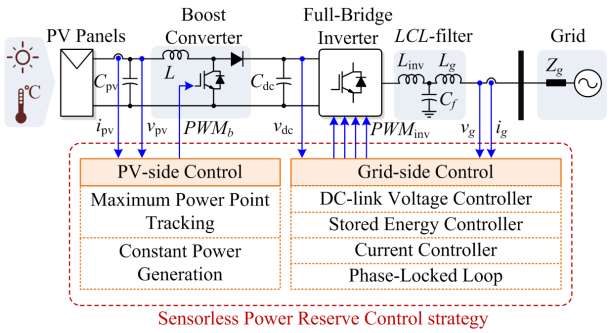

Fig. 3. System configuration and control structure of a two-stage grid-connected PV system with the Sensorless Power Reserve Control strategy.

delivers the extracted PV power to the ac grid by regulating the dc-link voltage v_{dc} to be constant through the control of the grid current i_{g} [28]. In this case, a bipolar Pulse Width Modulation (PWM) technique is used in order to eliminate the common-mode voltage, and thus minimize the leakage current [29]. This is a common requirement for transformerless PV applications. In addition, the grid-side converter also requires a proper synchronization of the injected current with the grid voltage by means of Phase-Locked Loops (PLL), and ensures the power quality of the injected grid-current with harmonic compensators being implemented.

In fact, the dc and ac power are decoupled in the two-stage configuration, where the dc-link capacitor acts as an energy buffer to decouple the dc and ac power. Thus, it is possible to adaptively adjust the stored energy in the dc-link to some extent during operation. In that case, the dc-link voltage is not always kept as constant in order to temporarily reserve the extracted power from the PV, which is the main idea of the proposed SPRC strategy and will be further discussed in details in the following.

III. Proposed Sensorless Power Reserve Control Strategy

A. Operational Principle

The proposed SPRC strategy is a combination of two operational modes: MPPT and CPG, which are employed for different control objectives. The main purpose of the MPPT operation is to estimate the available PV power. When the operating point of the PV arrays is regulated at the MPP, the available power of the PV arrays P_{avai} can be estimated from the measured PV output power P_{pv} (neglecting power losses due to the MPPT algorithm). By routinely assigning the MPPT operation, the available power can continuously be estimated during operation. In fact, this concept is similar to the "Sample and Hold (S&H)" process in digital control. Thus, similar consideration also applies here. That is, an error between the sampled signal (estimated available power) and the original signal (real available power) reduces as the sampling frequency increases (i.e., the more often the MPPT mode is assigned). This concept of the Available Power Estimation (APE) process is further illustrated in Figs. 4(a) and (b). In this way, the costly irradiance measurement or the PV panel characteristic models

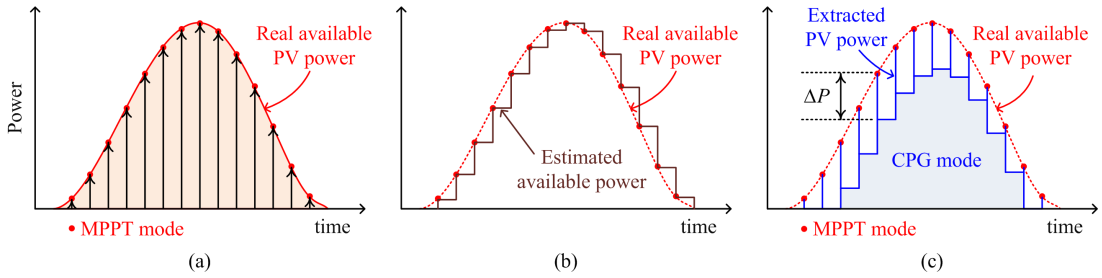

Fig. 4. Available power estimation method employed in the proposed Sensorless Power Reserve Control (SPRC) strategy: (a) MPPT mode is routinely employed, (b) the estimated available power during the MPPT mode, and (c) the extracted PV power with a combined MPPT and CPG operations.

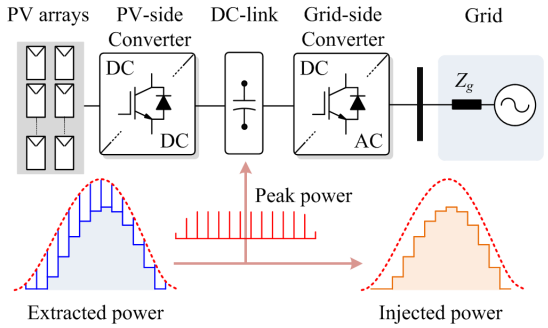

Fig. 5. Operational principle of the Sensorless Power Reserve Control (SPRC) strategy, where the peak power is stored/buffered in the dc-link during the MPPT mode (i.e., during the available power estimation period).

are not required for the available power estimation, being a sensorless solution.

Once the available PV power is estimated with the MPPT operation, the set-point of the CPG operation P_{limit} can be calculated according to (1), for a given amount of power reserve ΔP. Accordingly, the SPRC strategy employs the CPG operation to regulate the PV power in order to provide a power reverse as demanded. The corresponding extracted PV power from the dc-dc boost converter with the combination of MPPT and CPG modes is shown in Fig. 4(c). In order to ensure that the power injected to the ac grid always follows the demand in the case of the PRC shown in Fig. 1, the peak power during the MPPT mode should be buffered. In the proposed approach, the dc-link voltage is increased during this period to temporarily store the excessed energy due to the peak power injection. By doing so, the injected ac power will follow the PRC constraint as it is shown in Fig. 5. In this regard, the proposed solution can be flexibly adapted to any two-stage PV system configuration (with other PV inverter topologies), where the PV- and the grid-side converters can be controlled independently. The control algorithm of the PV-side boost converter and grid-side converter to achieve the discussed strategy is presented in the following.

B. Control Algorithm of the PV-Side Boost Converter

As discussed previously, there are two operating modes for the boost converter. Namely, the MPPT operation is employed to estimate the available PV power, and the CPG control is employed to regulate the PV output power to follow the power reserve demand. By combining both operating modes, the corresponding extracted PV power from the proposed strategy can be summarized as follows:

$$P_{\text{pv}} = \begin{cases} P_{\text{avai}} & \text{MPPT mode} \\ P_{\text{limit}} = P_{\text{avai}} - \Delta P & \text{CPG mode.} \end{cases} \tag{2}$$

Considering the MPPT mode, a fast MPPT operation is required in order to minimize the excessed energy injected into the dc-link during this APE period (i.e., ideally should be like an impulse). A simple and effective way to operate the PV system at the MPP is to use a Constant Voltage MPPT (CV-MPPT) strategy, where the PV voltage v_{pv} at the MPP can be approximated as 71-78 % of the open-circuit voltage V_{OC} [30], as illustrated in Fig. 6. Since the open-circuit voltage of the PV panels varies in a small range during operation, the CV-MPPT method offers a fast response with a moderate accuracy, making it suitable for implementation in the proposed SPRC strategy. The reference PV voltage v_{pv}^* during the MPPT mode can be assigned as follows:

$$v_{\text{pv}}^* = k_{\text{OC}} V_{\text{OC}}, \quad 0.71 < k_{\text{OC}} \leq 0.78, \tag{3}$$

where k_{OC} is a constant. Notably, the effectiveness of the CV-MPPT algorithm relies on the assumption that the voltage at the MPP does not change significantly during operation. This assumption is quite reasonable for this particular power reserve control (frequency response), where the required time duration is usually in the range of a few minutes [31]. In that short time period, the ambient temperature will not change significantly either (while the irradiance level could), as the ambient temperature usually changes with a time constant in the range of several minutes to an hour. Thus, it can be assumed that the impact of the temperature variation can be neglected during the power reserve control. That is to say, in the case of PRC operation, the ambient temperature is assumed to be constant. With the above MPPT operation, the available PV power can be estimated by simply measuring the PV power during the steady-state MPPT periods.

Once the APE process is done, the PV system enters into the CPG mode where the operating point of the PV systems has to be regulated below the MPP in order to achieve $P_{\text{pv}} = P_{\text{limit}}$ (and thus the power reserve). It can be seen from the P-V characteristic of the PV panel in Fig. 7 that there are two possible operating points for a certain level of P_{limit} and irradiance level (i.e., A and C). However, it should be aware that the operating point at the right side of the MPP (e.g., at

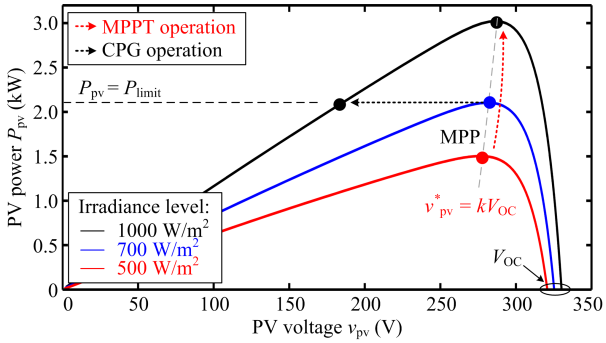

Fig. 6. Operational principle of the PV side control scheme, where the Constant Voltage MPPT and the CPG algorithms are implemented.

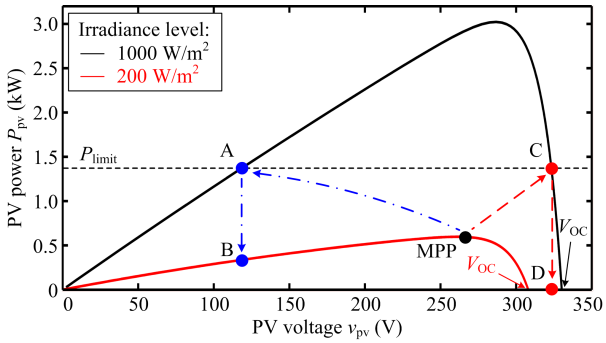

Fig. 7. Possible operating regions of the CPG strategy, where the instability issue during the fast decreasing irradiance condition is illustrated.

C) can introduce instability during a fast irradiance drop (e.g., from 1000 to 200 W/m^2 due to passing clouds). In that case, the open-circuit voltage of the PV panels V_{OC} decreases as the irradiance level drops, and the operating point may fall into (and stay at) the open-circuit condition (i.e., C→D in Fig. 7). Under this situation, the CPG operation becomes unstable and the PV system will not able to deliver any power from the PV panel to the grid, as it has been demonstrated in [17]. With this concern, the operating point of the PV system is perturbed to the left side of the MPP during the CPG opertion, as it is also illustrated in Fig. 6 [17]–[19]. The reference PV voltage v^*_{pv} during the CPG mode can be summarized as

$$v^*_{pv} = \begin{cases} v_{MPPT} & \text{when} \quad P_{pv} \le P_{limit} \\ v_{pv} - v_{step} & \text{when} \quad P_{pv} > P_{limit}, \end{cases} \tag{4}$$

where v_{MPPT} is the reference voltage from the MPPT algorithm (i.e., the P&O MPPT) and v_{step} is the perturbation step size. Notably, the reference v_{MPPT} has nothing to do with the previous CV-MPPT algorithm (which is only used during the APE process), but the v_{MPPT} is needed during the CPG operating mode in order to keep the operating point of the PV system at $P_{pv} = P_{limit}$. This is due to the fact that the PV power may not be kept exactly at the P_{limit} in practice, but it will oscillate around that operating point with minimum deviations. In that case, the PV voltage needs to follow the reference from the P&O MPPT algorithm when $P_{pv} \le P_{limit}$, in order to move the operating point back close to $P_{pv} = P_{limit}$. Further discussions about CPG algorithms can be found in [17]. The control structure of the PV-side boost converter is shown in Fig. 8,

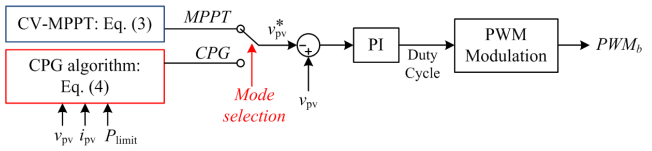

Fig. 8. Control scheme of the PV-side boost converter with the MPPT and CPG operation, where v^*_{pv} and v_{pv} are the reference and measured PV voltage, and P_{limit} is the set-point.

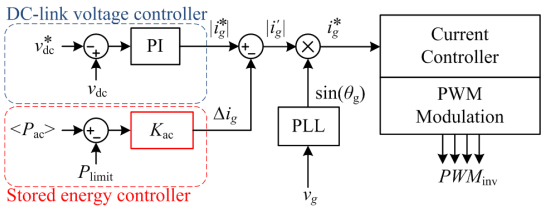

Fig. 9. Control scheme of the grid-side converter with the dc-link voltage controller and the stored energy controller, where v^*_{dc} and v_{dc} are the reference and measured dc-link voltage, $\langle P_{ac}\rangle$ is the average injected ac power, and P_{limit} is the set-point.

where a Proportional Integral (PI) controller is employed to regulate the PV voltage v_{pv} according to its reference v^*_{pv}. To avoid any confusion, due to the two operating modes (i.e., MPPT and CPG operations), the reference voltage v^*_{pv} in Fig. 8 is obtained from (3) during the APE process (MPPT operation), while the reference voltage in (4) is employed only during the CPG mode. In both cases, the control structure remains the same, while only the reference PV voltage v^*_{pv} is changed, as shown in Fig. 8.

C. Control Algorithm of the Grid-Side Converter

Regardless of the operating mode of the PV-side boost converter, the objective of the grid-side converter is to always keep the injected ac power to follow the PRC constraint as

$$\langle P_{ac}\rangle = P_{limit} = P_{avai} - \Delta P, \tag{5}$$

with $\langle P_{ac}\rangle$ being the average injected ac power, P_{limit} being the set-point (reference), P_{avai} being the available PV power, and ΔP being the required amount of reserved power.

In order to do so, the peak power during the APE period (i.e., MPPT mode) has to be temporarily stored in the dc-link. Following, the control scheme of the grid-side converter in Fig. 9 is employed in this paper, where a stored energy controller is plugged into the typical dc-link voltage controller for calculating the reference grid current. Basically, the dc-link voltage controller will give an amplitude reference of the grid current $|i^*_g|$, which keeps the dc-link voltage v_{dc} constant and delivers all the extracted PV power to the ac grid (which is the case during the CPG mode). However, if the average injected ac power $\langle P_{ac}\rangle$ exceeds the power limit P_{limit} (e.g., due to the peak power injection), a certain amount of current Δi_g corresponding to $k_{ac}(\langle P_{ac}\rangle - P_{limit})$ is subtracted from the reference $|i^*_g|$ by the stored energy controller. The proportional gain k_{ac} should be selected as $\sqrt{2}/V_g$ (with a small adjustment in practice to compensate power losses in the dc-link, e.g., parasitic resistance in the dc-link capacitor), where V_g is the

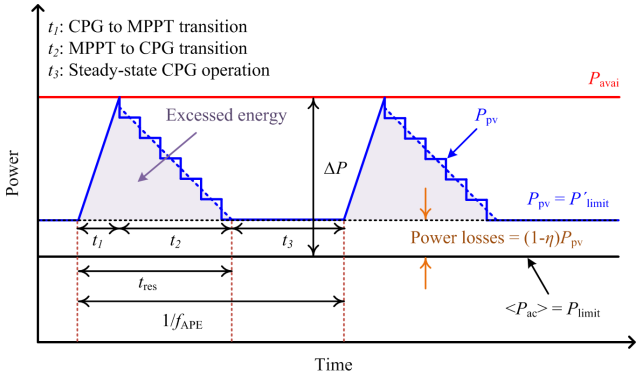

Fig. 10. Power extraction from the PV arrays according to the SPRC strategy with the power loss compensation, where t_{res} is the time response during the operating mode transition, f_{APE} is the sampling rate of the available PV power estimation process, and η is the efficiency of the power converter.

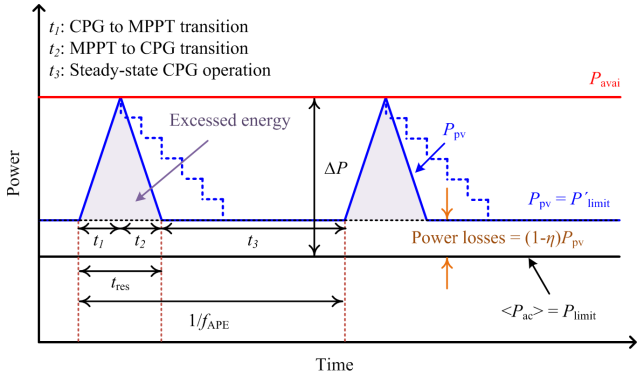

Fig. 11. Power extraction from the PV arrays according to the SPRC strategy with the previous operating point during the CPG mode being applied after the available PV power estimation process, where t_{res} is the time response during the operating mode transition, f_{APE} is the sampling rate of the available PV power estimation process, and η is the efficiency of the power converter.

RMS value of the grid voltage. In this way, the amount of the grid current reduction Δi_g, which will allow the power difference $(\langle P_{ac}\rangle - P_{limit})$ be stored in the dc-link, can be determined. Consequently, the actual dc-link voltage v_{dc} will be higher than the reference v^*_{dc} during the MPPT mode, but the peak power will not propagate to the ac grid.

In this approach, the stored energy in the dc-link is controlled indirectly through the compensation of the grid current, which offers a faster and more effective response than the solution by directly calculating the corresponding dc-link voltage (e.g., increase v^*_{dc} during MPPT operation). This is due to the typical limited bandwidth of the dc-link voltage controller (i.e., much slower than the current controller). Notably, v_{dc} should also be within a certain range for single-phase grid-connected inverter systems, in order to ensure the power delivery to the grid and safety (e.g., 400-600 V). Thus, there is a certain limit of the amount of reserved power ΔP in order to ensure that the dc-link voltage will not reach the system maximum voltage limit (e.g., 600 V) [32], [33], which will be discussed in the next section.

IV. Design Consideration of the SPRC Strategies

In order to achieve a high control performance using the SPRC strategy, several design considerations should be discussed to assist the practical implementations.

A. Improving the Power Reserve Accuracy by Compensating Inverter Power Losses

So far, the efficiency of the converters are not considered. In other words, it is assumed that the PV power P_{pv} in (2) is equal to the injected ac power $\langle P_{ac}\rangle$ in (5) during the CPG operation. However, there are power losses in the power converters, especially from the power devices during the switching and conduction, which reduces the converter efficiency. The power losses cannot be neglected and should be compensated, in order to achieve a high-accuracy operation.

Taking the efficiency of the power converter into account, the power injected to the grid from the PV arrays becomes

$$\langle P_{ac}\rangle = \eta \cdot P_{pv} \quad (6)$$

$$P_{pv} - \langle P_{ac}\rangle = (1-\eta)\cdot P_{pv}, \quad (7)$$

where η is the efficiency of the power converter. It can be observed in (7) that there is always a certain amount of power losses from the PV side to the grid side corresponding to $(1-\eta)\cdot P_{pv}$. In order to maintain the power reserve constraint with respect to the injected ac power as in (5), the amount $(1-\eta)\cdot P_{pv}$ should be subtracted from the reference ΔP when calculating the power limit as

$$P'_{limit} = P_{avai} - [\Delta P - (1-\eta)\cdot P_{pv}], \quad (8)$$

where P'_{limit} is the compensated power limit. By replacing the P_{limit} with P'_{limit} at the PV-side controller in (2) (while (5) remains), the power losses in the power converter are compensated, as it is illustrated in Fig. 10.

B. Minimizing the Excessed Energy with Fast CPG Algorithms during Transients

The key performance of the SPRC strategy is a fast operation during the available power estimation process in order to minimize the excessed energy in the dc-link. As it is shown in Fig. 10, there are two intermediate steps during this period: 1) CPG to MPPT (during t_1) and 2) MPPT to CPG (during t_2) transitions, where a certain time response t_{res} is required. With the CV-MPPT method discussed in Section III, the CPG to MPPT transition can be achieved very fast, where the reference $v^*_{pv} = k_{OC}V_{OC}$ is directly assigned. Thus, the remaining issue is to ensure a fast transient response of the CPG algorithm during the MPPT to CPG transition.

A simple and effective solution is to directly apply the last operating point during the steady-state CPG operation as a reference PV voltage once the APE process is done. In this way, the operating point of the PV can move back relatively fast to the previous operating point in the CPG mode within one sampling period. After that, the CPG algorithm in (4) is employed in steady-state CPG operation (during t_3). With this approach, the time response during the transition t_{res} is minimized, as it can be compared from t_{res} shown in Fig. 10 (with normal CPG algorithm, where a number of sampling during MPPT to CPG transition is required) and Fig. 11 (with fast CPG algorithm). This solution is effective when the

sampling rate of the APE process is much faster than the solar irradiance fluctuation, which is usually the case for the PV system in practice. Under this condition, it can be assumed that the operating point during the CPG mode for each sampling changes relatively slow, due to the high sampling rate of APE.

C. Maximum Amount of the Power Reserve

The maximum amount of power reserve ΔP_{max} is limited by the stored energy capacity of the dc-link capacitor. This is due to the fact that during each APE process, the excessed energy will be injected into the dc-link, which has a limited energy capacity. According to Fig. 11, the excessed energy during the APE process ΔE can be approximated as

$$\begin{aligned}\Delta E &= \frac{1}{2}(\Delta P - (1-\eta)\cdot P_{\text{pv}})t_{\text{res}} \\ &= \frac{1}{2}(P_{\text{avai}} - P'_{\text{limit}})t_{\text{res}}. \end{aligned} \quad (9)$$

When this excessed energy is stored in the dc-link, it will cause the dc-link voltage v_{dc} increase according to

$$\Delta E = \frac{1}{2}C_{\text{dc}}(v_{\text{dc,t}}^2 - v_{\text{dc,0}}^2), \quad (10)$$

where $v_{\text{dc,0}}$ is the initial dc-link voltage, which corresponds to the reference dc-link voltage v_{dc}^* in the SPRC strategy. $v_{\text{dc,t}}$ is the peak value of the dc-link voltage which is limited by the maximum allowable dc-link voltage $v_{\text{dc,max}}$ according to the grid regulations (e.g., 600 V in US [32] and 1000 V in Europe [33]). Thus, the maximum excessed energy that can be stored in the dc-link during each APE process is determined as follows:

$$\Delta E_{\text{max}} = \frac{1}{2}C_{\text{dc}}(v_{\text{dc,max}}^2 - v_{\text{dc}}^{*2}). \quad (11)$$

According to (9)-(11), the maximum amount of the power reserve ΔP_{max} is obtained as

$$\Delta P = \frac{C_{\text{dc}}}{t_{\text{res}}}(v_{\text{dc,t}}^2 - v_{\text{dc,0}}^2) + (1-\eta)\cdot P_{\text{pv}} \quad (12)$$

$$\Delta P_{\text{max}} = \frac{C_{\text{dc}}}{t_{\text{res}}}(v_{\text{dc,max}}^2 - v_{\text{dc}}^{*2}) + (1-\eta)\cdot P_{\text{pv}}. \quad (13)$$

It is noticed from (13) that, in order to increase ΔP_{max}, either a large dc-link capacitor C_{dc} is needed or the time response t_{res} has to be minimized. However, increasing the dc-link capacitance is usually not preferable considering the cost, size, and reliability of the system [34]. In this paper, the dc-link capacitance C_{dc} is designed based on the maximum ripple voltage Δv requirement during normal operation, where the dc-link capacitance is determined by

$$C_{\text{dc}} = \frac{P_{\text{pv}}}{(2\pi f_g)\cdot \Delta v \cdot v_{\text{dc}}}. \quad (14)$$

At the rated power (i.e., 3 kW), the dc-link voltage is regulated at 450 $\pm$ 5 V (i.e., v_{dc} = 450 V, Δv = 5 V). Thus, the required dc-link capacitance is around 2.2 mF according to (14). Notably, this is a typical design for single-phase inverter, where the dc-link voltage inevitably contains the double-line frequency ripples during operation. This dc-link capacitor however can be used to store the excessive energy in the SPRC operation. In other words, the dc-link capacitor is not oversized or specifically designed for the power reserve purpose. Consequently, from this standpoint, reducing the time response t_{res} is a more viable solution to maximize the power reserve of a pre-designed two-stage PV system according to (13).

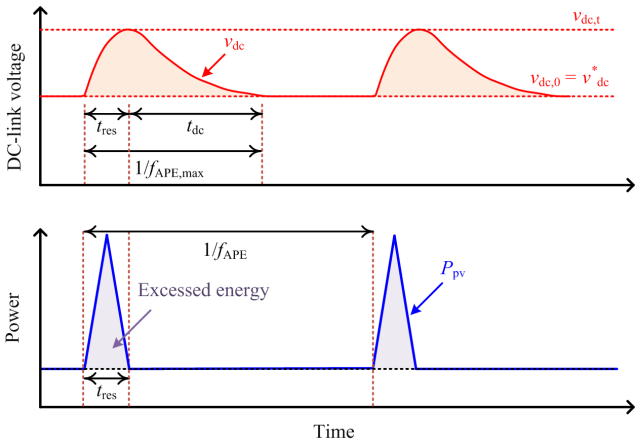

Fig. 12. Variation in the dc-link voltage due to the peak power injection during the MPPT mode, where t_{res} and t_{dc} are the time response during the operating mode transition and the dc-link voltage controller, respectively. f_{APE} is the sampling rate of the APE process and $f_{\text{APE,max}}$ is its maximum value.

D. Maximum Sampling Frequency of the Available Power Estimation (APE) Process

The accuracy of the APE relies on its sampling frequency f_{APE}. In general, the accuracy of the APE increases as its sampling rate f_{APE} increases, especially during the changing irradiance condition. However, the constraint that limits the sampling frequency f_{APE} is the required response time by the dc-link voltage controller in order to reach the steady-state after the peak power injection due to the APE process. Specifically, the dc-link voltage has to be discharged to its nominal value (i.e., $v_{\text{dc}} = v_{\text{dc}}^*$) at the end of each APE sampling. Otherwise, if the excessed energy is injected to the dc-link during the discharging period, the dc-link voltage will oscillate. This will lead to an unstable operation, since the boost converter can no longer regulate its input voltage (i.e., PV voltage) when the output voltage (i.e., dc-link voltage) is oscillating significantly, as it will be exemplified later via experiments. The variation in the dc-link voltage v_{dc} during each APE process is illustrated in Fig. 12. At the beginning of each APE process, the dc-link voltage will reach its peak value after $t = t_{\text{res}}$, which is the time duration where the excessed energy is injected into the dc-link. After that, the dc-link voltage will be slowly discharged by the dc-link voltage controller. During this period, the stored energy controller is deactivated, since $(\langle P_{\text{ac}}\rangle - P_{\text{limit}}) = 0$. Thus, the required discharging time t_{dc} corresponds to the settling time of the dc-link voltage controller (e.g., the PI controller), and the maximum sampling frequency of the APE process $f_{\text{APE,max}}$ can be obtained as

$$f_{\text{APE,max}} = \frac{1}{t_{\text{res}} + t_{\text{dc}}}. \quad (15)$$

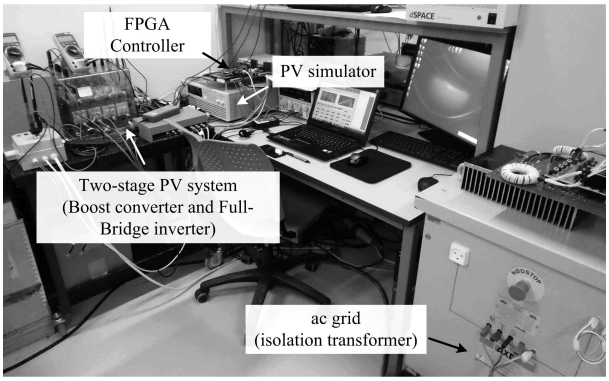

Fig. 13. Experimental setup of the two-stage grid-connected PV system.

TABLE I
PARAMETERS OF THE TWO-STAGE SINGLE-PHASE PV SYSTEM (FIG. 3).

PV rated power	3 kW
Boost converter inductor	L = 1.8 mH
PV-side capacitor	C_{pv} = 1000 μF
DC-link capacitor	C_{dc} = 2200 μF
LCL-filter	L_{inv} = 4.8 mH, L_{g} = 2 mH, C_f = 4.3 μF
Switching frequency	Boost converter: f_b = 16 kHz, Full-Bridge inverter: f_{inv} = 8 kHz
DC-link voltage	V_{dc} = 400-600 V
Grid nominal voltage (RMS)	V_g = 230 V
Grid nominal frequency	ω_0 = 2π×50 rad/s

V. PERFORMANCE VERIFICATION OF THE PROPOSED SPRC STRATEGIES

In order to verify the effectiveness of the proposed SPRC strategy, the experimental tests have been carried out with the test-rig shown in Fig. 13, where the system parameters are given in Table I. It should be pointed out that an LC-filter is used, and connected to the grid through an isolation transformer. Together with the leakage inductance of the isolation transformer, an LCL-filter is formed. At the PV-side, a PV simulator has been adopted. The control algorithms have been implemented in an FPGA system.

First, a constant solar irradiance profile of 1000 W/m^2 (i.e., corresponding to the available PV power of 3 kW) has been adopted in the test. In this case, three power reserve references ΔP (i.e., 700 W, 500 W, and 300 W) are used to verify the effectiveness of the SPRC strategy during steady-state operation, and the results are shown in Fig. 14. The PV voltage v_{pv} and the corresponding extracted PV power P_{pv} are shown in Figs. 14(a) and (b), respectively. During the CPG operation periods, the extracted PV power P_{pv} is limited below the available power P_{avai} corresponding to the amount of the power reserve ΔP, while the PV power reaches the available power during the MPPT mode. At the grid-side, the average injected ac power $\langle P_{\text{ac}} \rangle$ always follows the PRC constraint during operation, as it can be seen in Fig. 14(b). This is achieved by the stored energy controller, where the dc-link voltage v_{dc} is adaptively controlled to absorb the peak

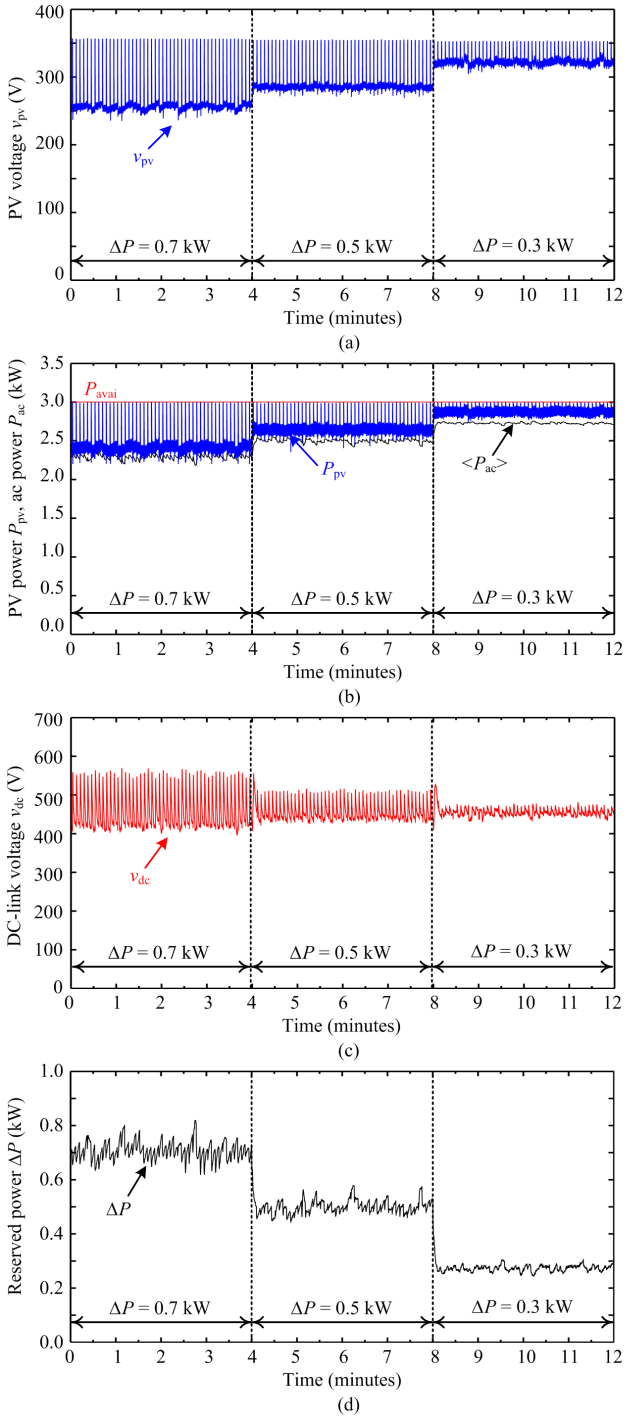

Fig. 14. Experimental results of the single-phase grid-connected PV system with the proposed SPRC strategy during the steady-state operation (solar irradiance level: 1000 W/m^2; ambient temperature: 25°C; available power estimation rate: f_{APE} = 0.2 Hz), where the reference power reserve ΔP are 700 W, 500 W, and 300 W: (a) PV voltage v_{pv}, (b) PV power P_{pv} and ac power $\langle P_{\text{ac}} \rangle$, (c) dc-link voltage v_{dc}, and (d) reserved power ΔP.

power injection in the dc-link during the MPPT mode. It can be noticed in Fig. 14(c) that the variation in the dc-link voltage increases as the amount of power reserve increases, while the average value remains the same. More specifically, the dc-link voltage only increases temporarily during the APE process in order to store the excessed energy in the dc-link. In this case,

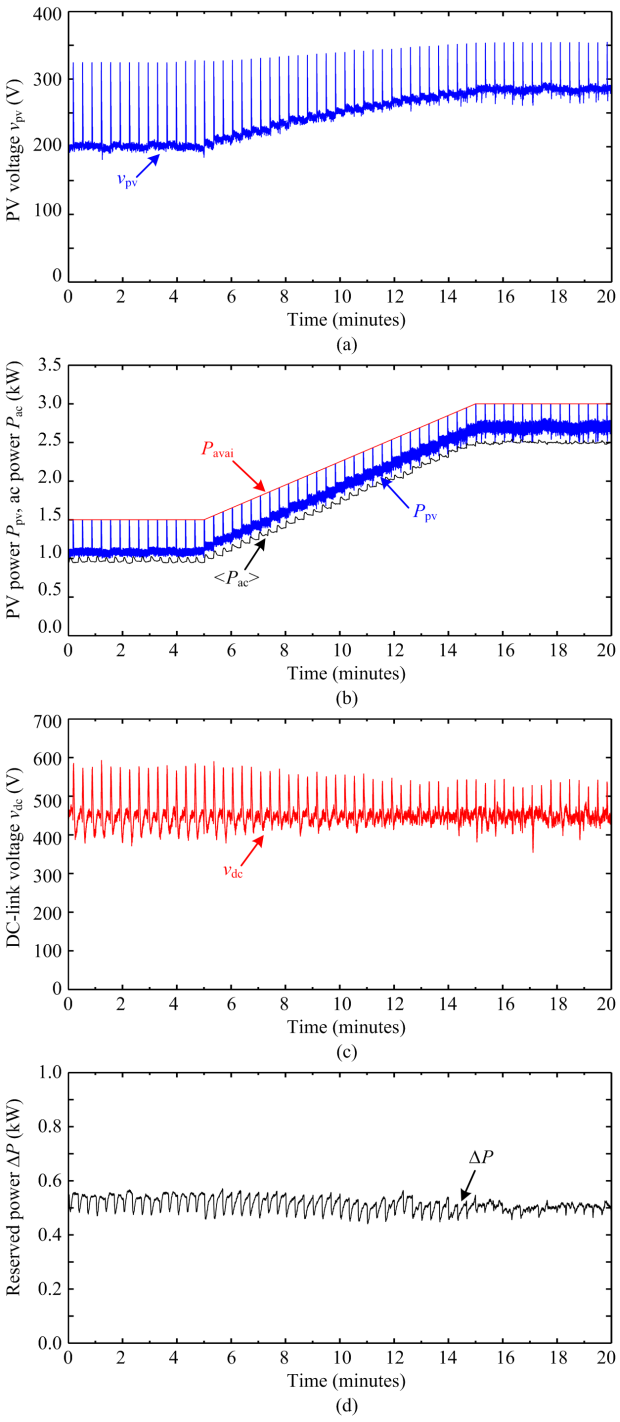

Fig. 15. Experimental results of the single-phase grid-connected PV system with the proposed SPRC strategy at the sampling rate of f_{APE} = 0.05 Hz under a ramp-changing solar irradiance profile (ambient temperature: 25°C), where the reference power reserve ΔP is 500 W: (a) PV voltage v_{pv}, (b) PV power P_{pv} and ac power $\langle P_{\mathrm{ac}} \rangle$, (c) dc-link voltage v_{dc}, and (d) reserved power ΔP.

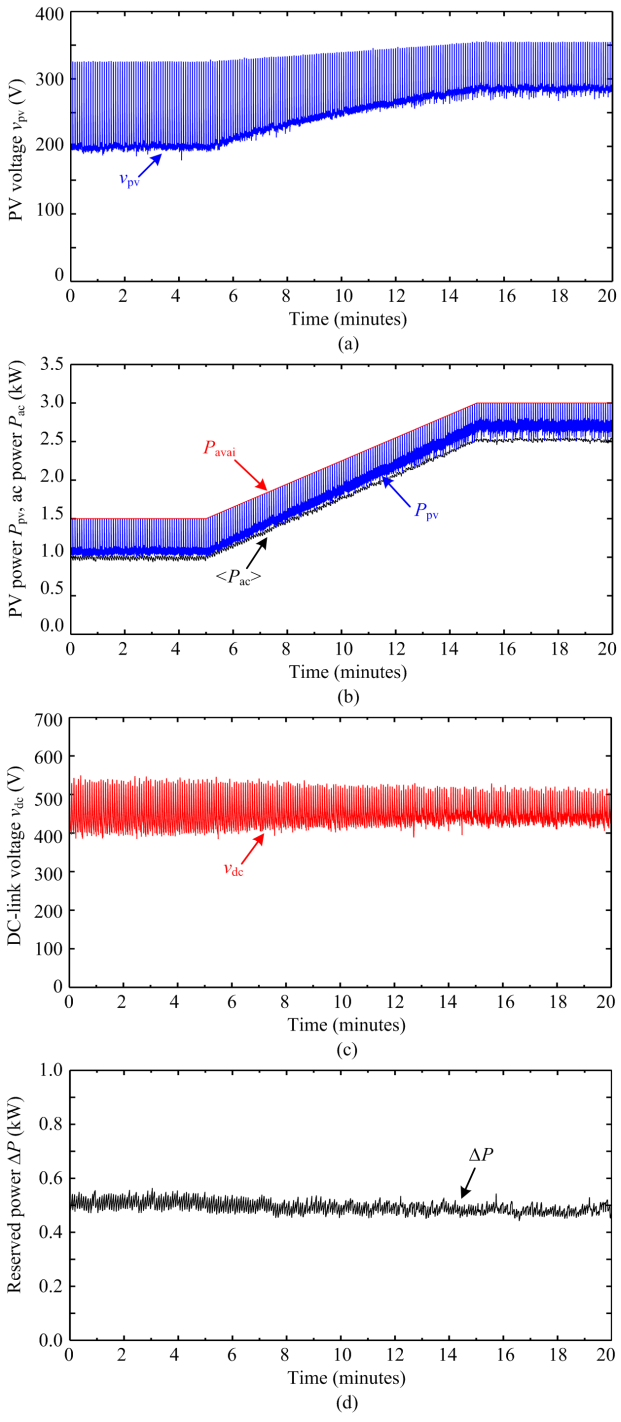

Fig. 16. Experimental results of the single-phase grid-connected PV system with the proposed SPRC strategy at the sampling rate of f_{APE} = 0.2 Hz under a ramp-changing solar irradiance profile (ambient temperature: 25°C), where the reference power reserve ΔP is 500 W: (a) PV voltage v_{pv}, (b) PV power P_{pv} and ac power $\langle P_{\mathrm{ac}} \rangle$, (c) dc-link voltage v_{dc}, and (d) reserved power ΔP.

the peak dc-link voltage is highest when the power reserve is 700 W, as it can be seen from Fig. 14. This is in a close agreement with the previous theoretical analysis according to (12). Nevertheless, the average reserved power ΔP can be accurately controlled according to the references, as it is shown in Fig. 14(d).

Further, the proposed SPRC strategy has also been verified with a ramp-changing irradiance profile, where the performance of the APE process becomes important. As mentioned previously, the accuracy of the APE process relies on its sampling rate f_{APE}. Thus, two different sampling frequencies of f_{APE} = 0.05 Hz and 0.2 Hz are used in this test, while

the reference power reserve ΔP is kept as 500 W. The performances of the SPRC with a low sampling frequency of APE process are shown in Fig. 15. The PV voltage v_{pv} under this operating condition is shown in Fig. 15(a), where it can be seen that the MPPT operation is assigned to the boost converter every 20 s (i.e., $f_{\text{APE}} = 0.05$ Hz). In Fig. 15(b), the available PV power P_{avai} and the extracted PV power P_{pv} during operation are shown, which demonstrates that the available power P_{avai} is periodically measured in the MPPT mode. The injected ac power $\langle P_{\text{ac}} \rangle$ during operation is also shown in the same figure, where it can be observed that the power reserve constraint is achieved. However, a power reserve profile ΔP in Fig. 15(d) presents a considerable error during operation due to the low sampling rate of the APE process.

In order to reduce the power reserve error and demonstrate the impact of the sampling frequency of the APE process f_{APE} on the performance of the SPRC strategy, a high sampling rate of 0.2 Hz for the APE process is adopted in Fig. 16. In this case, the MPPT operation is assigned to the boost converter every 5 s (i.e., $f_{\text{APE}} = 0.2$ Hz). This can be noticed from the PV voltage v_{pv} in Fig. 16(a), where the CV-MPPT algorithm is assigned more frequently compared to that in Fig. 15(a). A similar high frequency transition between the MPPT and CPG mode is also observed in the extracted PV power P_{pv} in Fig. 16(b). On the other hand, the injected ac power $\langle P_{\text{ac}} \rangle$ fluctuation is reduced with this high sampling rate due to the higher accuracy in the available power estimation. Consequently, the error in the reserved power ΔP is significantly reduced, as it can be seen from Fig. 16(d).

A zoomed-in view of the experimental results (in Fig. 16) is presented in Fig. 17, where the PV system is operating with a constant available power of 3 kW. Here, it can be observed from the PV voltage v_{pv} in Fig. 17(a) that the algorithm can reach the MPP very fast with the CV-MPPT operation, where the response time t_{res} during the operational mode transition (i.e., CPG→MPPT→CPG) is around 0.5 s. Notably, this is much faster than the typical required response time during the power reserve operation in the grid code, i.e., 10 s in the Danish grid code [7]. The extracted PV power P_{pv} and the injected ac power $\langle P_{\text{ac}} \rangle$ are also shown in Fig. 17(b), where the power losses from dc to ac in the steady-state is around 180 W. Fig. 17(c) shows the zoomed-in view of the dc-link voltage v_{dc}, where it can be seen that the dc-link voltage increases during the peak power injection, similar to what has been discussed in Fig. 12. In the same figure, the response time of the dc-link voltage has also been measured as $t_{\text{dc}} = 2$ s.

In fact, the variations in the dc-link during each APE process can be estimated as in (12). For instance, considering the APE process in the above experimental tests, the initial value of the dc-link voltage $v_{\text{dc,0}}$ is around 440 V. The peak value of the dc-link voltage $v_{\text{dc,t}}$ can be estimated following

$$\begin{aligned} \Delta P &= \frac{C_{\text{dc}}}{t_{\text{res}}}\left(v_{\text{dc,t}}^2 - v_{\text{dc,0}}^2\right) + (1-\eta)\cdot P_{\text{pv}} \\ v_{\text{dc,t}} &= \sqrt{\left[\Delta P - (1-\eta)\cdot P_{\text{pv}}\right]\frac{t_{\text{res}}}{C_{\text{dc}}} + v_{\text{dc,0}}^2} \\ v_{\text{dc,t}} &= \sqrt{\left[500 - 180\right]\frac{0.5}{2.2\cdot 10^{-3}} + 440^2} = 516 \text{ V}, \end{aligned}$$

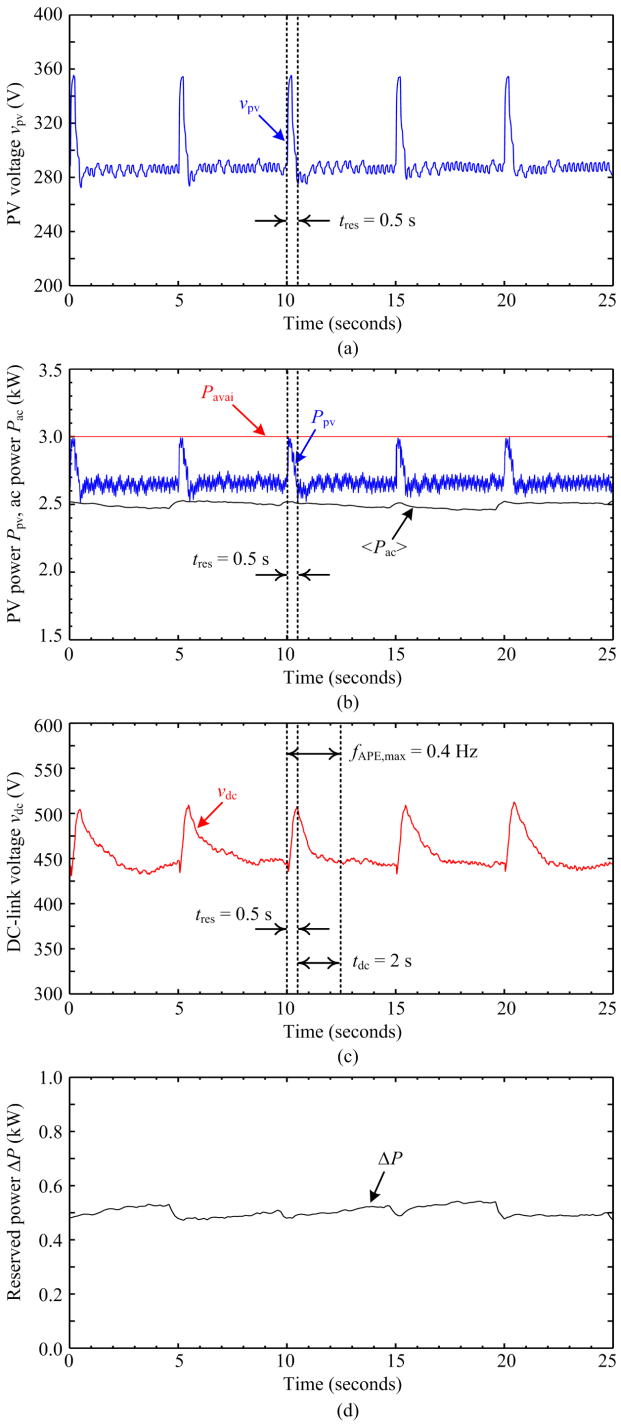

Fig. 17. Zoomed-in view of the results in Fig. 16: (a) PV voltage v_{pv}, (b) PV power P_{pv} and ac power $\langle P_{\text{ac}} \rangle$, (c) dc-link voltage v_{dc}, (d) reserved power ΔP.

which closely agrees with the peak value of the measured dc-link voltage in Fig. 17(c). The peak value of the dc-link voltage is also measured at other power reserve levels and compared with the calculation in (12), where the system parameters are kept the same (i.e., $t_{\text{res}} = 0.5$ s, $C_{\text{dc}} = 2.2$ mF, $v_{\text{dc,0}} = 440$ V). The analysis in Section IV is verified with the results in Fig. 18, where only small errors between the measured and the calculated peak value of the dc-link voltage are observed.

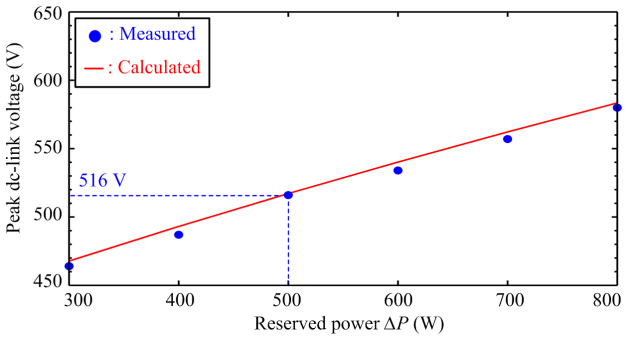

Fig. 18. Peak value of the dc-link voltage according to different power reserved levels, when t_{res} = 0.5 s, C_{dc} = 2.2 mF, $v_{dc,0}$ = 440 V.

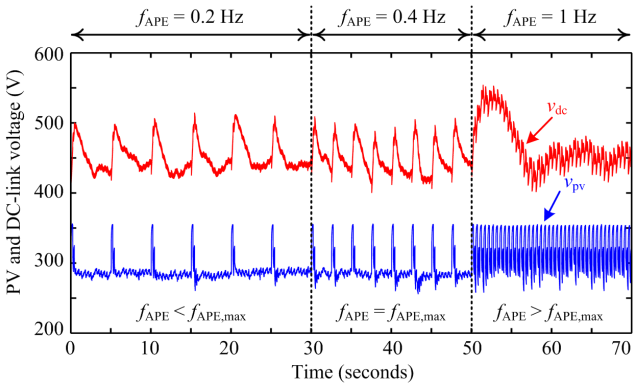

Fig. 19. Experimental result of the PV voltage v_{pv} and the dc-link voltage v_{dc} with different available power estimation sampling rates f_{APE}.

From the measured time respond t_{res} and t_{dc} in Figs. 17(a) and (c), the maximum sampling frequency of the APE process $f_{APE,max}$ can be calculated as follows:

$$f_{APE,max} = \frac{1}{t_{res} + t_{dc}} = \frac{1}{0.5 + 2} = 0.4 \text{ Hz}.$$

This operational boundary has also been verified experimentally, where three cases of the APE sampling rate are adopted: $f_{APE} < f_{APE,max}$, $f_{APE} = f_{APE,max}$, and $f_{APE} > f_{APE,max}$. It can be seen from the dc-link voltage v_{dc} in Fig. 19 that the dc-link voltage increases almost immediately after it reaches the initial value (i.e., 440 V) when the maximum sampling rate is adopted (i.e., $f_{APE} = f_{APE,max}$). When the sampling rate of the APE process is further increased above the maximum limit (i.e., $f_{APE} > f_{APE,max}$), the average dc-link voltage continuously increases during the transient and oscillates during the steady-state. In this case, it can also be seen from the PV voltage that the operating transition between the CPG and MPPT is not achievable, as it becomes difficult for the boost converter to control its input voltage (PV voltage) when the output voltage (dc-link voltage) is oscillating [35]. Thus, exceeding the maximum sampling rate of the APE process can lead to over-voltage in the dc-link and also unstable PRC operation, which should be avoided.

VI. Conclusion

A cost-effective sensorless power reserve control strategy for two-stage grid-connected PV systems has been proposed in this paper. The cost-effectiveness of the proposal lies in the sensorless estimation of the available PV power, which is achieved by routinely employing a fast MPPT operation. Then, the estimated available power is used for calculating the set-point to limit the extracted PV power with the CPG operation. At the grid-side, the stored energy in the dc-link is adaptively controlled to minimize the power fluctuation during the available PV power estimation process, where the excessed energy is temporarily stored in the dc-link. With the above coordinated control strategy, the power reserve control can be achieved as it has been verified experimentally. Design considerations for a high control performance and the operational boundary have also been discussed to assist the practical implementations.

References

[1] REN21, "Renewables 2016: Global Status Report (GRS)," 2016. [Online]. Available: http://www.ren21.net/.

[2] Fraunhofer ISE, "Recent Facts about Photovoltaics in Germany," April 22, 2016. [Online]. Available: http://www.pv-fakten.de/.

[3] Solar Power Europe, "Global Market Outlook For Solar Power 2015 - 2019," 2015. [Online]. Available: http://www.solarpowereurope.org/.

[4] E. Reiter, K. Ardani, R. Margolis, and R. Edge, "Industry perspectives on advanced inverters for us solar photovoltaic systems: Grid benefits, deployment challenges, and emerging solutions," National Renewable Energy Laboratory (NREL), Tech. Rep. No. NREL/TP-7A40-65063., 2015.

[5] Y. Yang, P. Enjeti, F. Blaabjerg, and H. Wang, "Wide-scale adoption of photovoltaic energy: Grid code modifications are explored in the distribution grid," *IEEE Ind. Appl. Mag.*, vol. 21, no. 5, pp. 21–31, Sep. 2015.

[6] BDEW, "Technische richtlinie erzeugungsanlagen am mittelspannungsnetz - richtlinie fur anschluss und parallelbetrieb von erzeugungsanlagen am mittelspannungsnetz," Jun. 2008.

[7] Energinet.dk, "Technical regulation 3.2.2 for PV power plants with a power output above 11 kW," Tech. Rep. Doc. 14/17997-39, 2015.

[8] E. Troester, "New German grid codes for connecting PV systems to the medium voltage power grid," in *Proc. of 2nd Int. Workshop Concentrating Photovoltaic Power Plants: Opt. Design, Prod., Grid Connection*, pp. 1–4, 2009.

[9] B. I. Craciun, T. Kerekes, D. Sera, and R. Teodorescu, "Overview of recent grid codes for PV power integration," in *Proc. of OPTIM*, pp. 959–965, May 2012.

[10] A. Hoke, E. Muljadi, and D. Maksimovic, "Real-time photovoltaic plant maximum power point estimation for use in grid frequency stabilization," in *Proc. of COMPEL*, pp. 1–7, July 2015.

[11] B. I. Craciun, T. Kerekes, D. Sera, and R. Teodorescu, "Frequency support functions in large PV power plants with active power reserves," *IEEE J. Emerg. Sel. Topics Power Electron.*, vol. 2, no. 4, pp. 849–858, Dec. 2014.

[12] S. Nanou, A. Papakonstantinou, and S. Papathanassiou, "Control of a PV generator to maintain active power reserves during operation," in *Proc. of EU PVSEC*, pp. 4059–4063, 2012.

[13] N. Kakimoto, S. Takayama, H. Satoh, and K. Nakamura, "Power modulation of photovoltaic generator for frequency control of power system," *IEEE Trans. Energy Convers.*, vol. 24, no. 4, pp. 943–949, Dec. 2009.

[14] H. Beltran, E. Bilbao, E. Belenguer, I. Etxeberria-Otadui, and P. Rodriguez, "Evaluation of storage energy requirements for constant production in PV power plants," *IEEE Trans. Ind. Electron.*, vol. 60, no. 3, pp. 1225–1234, Mar. 2013.

[15] J. V. Appen, T. Stetz, B. Idlbi, and M. Braun, "Enabling high amounts of PV systems in low voltage grids using storage systems," in *Proc. of EU PVSEC*, pp. 2380–2386, 2014.

[16] E. Romero-Cadaval, B. Francois, M. Malinowski, and Q. C. Zhong, "Grid-connected photovoltaic plants: An alternative energy source, replacing conventional sources," *IEEE Ind. Electron. Mag.*, vol. 9, no. 1, pp. 18–32, Mar. 2015.

[17] A. Sangwongwanich, Y. Yang, F. Blaabjerg, and H. Wang, "Benchmarking of constant power generation strategies for single-phase grid-connected photovoltaic systems," in *Proc. of APEC*, pp. 370–377, Mar. 2016.

[18] A. Sangwongwanich, Y. Yang, and F. Blaabjerg, "High-performance constant power generation in grid-connected PV systems," *IEEE Trans. Power Electron.*, vol. 31, no. 3, pp. 1822–1825, Mar. 2016.
[19] L. D. Watson and J. W. Kimball, "Frequency regulation of a microgrid using solar power," in *Proc. of APEC*, pp. 321–326, Mar. 2011.
[20] S. Mishra, P. P. Zarina, and P. C. Sekhar, "A novel controller for frequency regulation in a hybrid system with high PV penetration," in *Proc. of IEEE Power Energy Soc. Gen. Meet*, pp. 1–5, July 2013.
[21] Y. Yang, H. Wang, F. Blaabjerg, and T. Kerekes, "A hybrid power control concept for PV inverters with reduced thermal loading," *IEEE Trans. Power Electron.*, vol. 29, no. 12, pp. 6271–6275, Dec. 2014.
[22] D. Premm, B. Osterkamp, J. Seidel, S. Poehling, A. Unru, and B. Engel, "The PV-Regel project - development of concepts and solutions for the provision of control reserve with PV," in *Proc. of EU PVSEC*, pp. 3124–3128, 2015.
[23] H. Xin, Z. Lu, Y. Liu, and D. Gan, "A center-free control strategy for the coordination of multiple photovoltaic generators," *IEEE Trans. Smart Grid.*, vol. 5, no. 3, pp. 1262–1269, May 2014.
[24] A. Sangwongwanich, Y. Yang, and F. Blaabjerg, "Sensorless reserved power control strategy for two-stage grid-connected photovoltaic systems," in *Proc. of PEDG*, pp. 1–8, June 2016.
[25] Y. T. Tan, "Impact on the power system with a large penetration of photovoltaic generation," Ph.D. dissertation, Dept. Electr. Electron. Eng., Univ. Manchester Inst. Sci. Technol., Manchester, U.K., Feb. 2004.
[26] N. A. Rahim, R. Saidur, K. H. Solangi, M. Othman, and N. Amin, "Survey of grid-connected photovoltaic inverters and related systems," *Clean Technol. Environ. Policy*, vol. 14, no. 4, pp. 521–533, 2012.
[27] Y. Yang and F. Blaabjerg, "Overview of single-phase grid-connected photovoltaic systems," *Electr. Power Componen. and Syst.*, vol. 43, no. 12, pp. 1352–1363, 2015.
[28] F. Blaabjerg, R. Teodorescu, M. Liserre, and A.V. Timbus, "Overview of control and grid synchronization for distributed power generation systems," *IEEE Trans. Ind. Electron.*, vol. 53, no. 5, pp. 1398–1409, Oct. 2006.
[29] R. Gonzalez, J. Lopez, P. Sanchis, and L. Marroyo, "Transformerless inverter for single-phase photovoltaic systems," *IEEE Trans. Power Electron.*, vol. 22, no. 2, pp. 693–697, March 2007.
[30] T. Esram and P.L. Chapman, "Comparison of photovoltaic array maximum power point tracking techniques," *IEEE Trans. Energy Convers.*, vol. 22, no. 2, pp. 439–449, Jun. 2007.
[31] European Network of Transmission System Operators for Electricity, "Network code for requirements for grid connection applicable to all generators," Tech. Rep., Mar. 2013. [Online]. Available: https://www.entsoe.eu.2013
[32] *National Electrical Code: 2008*. National Fire Protection Association, 2007.
[33] *IEC 61730: Photovoltaic (PV) module safety qualification*. International Electrotechnical Commission, 2016.
[34] H. Wang and F. Blaabjerg, "Reliability of capacitors for dc-link applications in power electronic converters - an overview," *IEEE Trans. Ind. Appl.*, vol. 50, no. 5, pp. 3569–3578, Sept. 2014.
[35] N. Mohan, T. M. Undeland, and W. P. Robbins, *Power electronics: converters, applications, and design*. New York: John Wiley and Sons, 2003.

Ariya Sangwongwanich (S'15) was born in Bangkok, Thailand, in 1991. He received the B.Eng. degree in electrical engineering from Chulalongkorn University, Thailand, in 2013, and the M.Sc. in energy engineering from Aalborg University, Denmark, in 2015, where he is currently working towards his Ph.D. degree. His research interests include control of grid-connected converter, photovoltaic systems, and high-power multilevel converters.

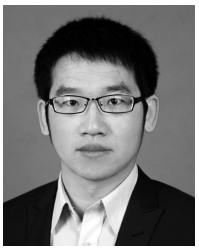

Yongheng Yang (S'12-M'15) received the B.Eng. degree in 2009 from Northwestern Polytechnical University, China and the Ph.D. degree in 2014 from Aalborg University, Denmark.

He was a postgraduate with Southeast University, China, from 2009 to 2011. In 2013, he was a Visiting Scholar with Texas A&M University, USA. Since 2014, he has been with the Department of Energy Technology, Aalborg University, where currently he is an Assistant Professor. His research interests are focused on grid integration of renewable energy systems, power converter design, analysis and control, harmonics identification and mitigation, and reliability in power electronics. Dr. Yang has published more than 80 technical papers and co-authored a book - *Periodic Control of Power Electronic Converters* (London, UK: IET).

Dr. Yang is a Member of the IEEE Power Electronics Society (PELS) Students and Young Professionals Committee. He served as a Guest Associate Editor of IEEE JOURNAL OF EMERGING AND SELECTED TOPICS IN POWER ELECTRONICS and a Guest Editor of *Applied Sciences*. He is an active reviewer for relevant top-tier journals.

Frede Blaabjerg (S'86-M'88-SM'97-F'03) was with ABB-Scandia, Randers, Denmark, from 1987 to 1988. From 1988 to 1992, he was a Ph.D. Student with Aalborg University, Aalborg, Denmark. He became an Assistant Professor in 1992, Associate Professor in 1996, and Full Professor of power electronics and drives in 1998. His current research interests include power electronics and its applications such as in wind turbines, PV systems, reliability, harmonics and adjustable speed drives.

He has received 18 IEEE Prize Paper Awards, the IEEE PELS Distinguished Service Award in 2009, the EPE-PEMC Council Award in 2010, the IEEE William E. Newell Power Electronics Award 2014 and the Villum Kann Rasmussen Research Award 2014. He was an Editor-in-Chief of the IEEE TRANSACTIONS ON POWER ELECTRONICS from 2006 to 2012. He was nominated in 2014, 2015 and 2016 by Thomson Reuters to be between the most 250 cited researchers in Engineering in the world.